Article

Reevaluating Mare Moscoviense And Its Vicinity Using Chang'e-2 Microwave Sounder Data

Zhiguo Meng [1,2,3,4], **Shengbo Chen** [1], **Yongzhi Wang** [1,2,3,*], **Tianxing Wang** [2],
Zhanchuan Cai [3], **Yuanzhi Zhang** [4], **Yongchun Zheng** [4] and **Shuo Hu** [1]

1   College of Geoexploration Science and Technology, Jilin University, Changchun 130026, China;
    mengzg@jlu.edu.cn (Z.M.); chensb@jlu.edu.cn (S.C.); hushuo17@mails.jlu.edu.cn (S.H.)
2   State Key Laboratory of Remote Sensing Science, Institute of Remote Sensing and Digital Earth, Chinese
    Academy of Sciences, Beijing 100101, China; wangtx@radi.ac.cn
3   State Key Laboratory of Lunar and Planetary Sciences, Macau University of Science and Technology,
    Macau, China; zccai@must.edu.mo
4   Key Laboratory of Lunar and Deep-space Exploration, National Astronomical Observatories, Chinese
    Academy of Sciences, Beijing 100101, China; zhangyz@nao.cas.cn (Y.Z.); zyc@nao.cas.cn (Y.Z.)
*   Correspondence: wangyongzhi@jlu.edu.cn; Tel.: +86-4318-850-2362

✓ check for updates

Abstract: Mare Moscoviense (148°E, 27°N) is one of the few large maria on the lunar farside, with the thinnest crust and a positive gravity anomaly. In this paper, the Chang'E-2 Microwave Sounder (CELMS) data was employed to study the microwave thermal emission features of mare basalts in Moscoviense Basin. The time angle and linear interpolation method are used to generate the brightness temperature (T_B) maps at noon and night, as well as the T_B difference (dT_B) map. The obtained important results are as follows. (1) A new geologic map is generated with the T_B and dT_B maps using the maximum likelihood method, which gives a new expression about the basaltic units in Mare Moscoviense compared to the optical results; (2) the substrate temperature of Moscoviense Basin is likely warmer than what we know; (3) unit Ihtm (a Late (?) Imbrian, mid- to high-Ti, high-Fe basalt) is re-understood as two independent volcanic features with their own fissures; (4) the dT_B maps firstly indicate that the depth lunar regolith is homogeneous in the highlands surrounding Mare Moscoviense, at least in the microwave domain, and secondly that there exists a special material bringing about the low dT_B anomaly in the shallow layer of the east highlands. The results will be of great significance to better understand the basaltic volcanism of the Moon.

Keywords: Mare Moscoviense; microwave thermal emission; basaltic units; basaltic volcanism; CELMS data

1. Introduction

Moscoviense Basin, centered at (148.12°E, 27.28°N), is a multi-ringed impact basin on the lunar farside located within the Feldspathic Highland Terrain (Figure 1a). It hosts abundant mare deposits, which cover an area of 35,000 km^2 within the 420 km diameter basin (Figure 1b) [1–4]. It was reported that Mare Moscoviense has some of the thinnest crust on the entire Moon and a large positive gravity anomaly for a basin in this size [5–7]. Therefore, observations and studies of the lunar regolith in Moscoviense Basin with the passive microwave data will be of great significance to improve understanding the basaltic volcanism on the lunar farside.

Up to now, five different volcanic units across the Basin were recognized, which were mainly based on spectral properties and composition, namely, high-Ti basalts, low-Ti basalts, ancient mare units, cryptomare, and highland basin soils [8,9]. Using Clementine data, Craddock et al. [10] revealed the unique, complex nature of the geology in Mare Moscoviense and found the evidence for large-scale

pyroclastic material on the northern lunar farside through the analysis of compositions and the ages of basalt units. Mainly dependent on the iron and titanium abundances (FTA) (Figure 1c), Mare Moscoviense is divided into four broad units, namely: Im (an Early(?) Imbrian, very low-Ti, low-Fe basalt), Iltm (an Imbrian-age, low-Ti, mare basalt), Ikm (an Imbrian low-Ti basalt that partially fills the crater Komarov), and Ihtm (a Late(?) Imbrian, mid- to high-Ti, high-Fe basalt) by Kramer et al. [9] or named Ehtm (Eratosthenian mid to high-Ti, high-Fe basalt) by Morota et al. [11] (Figure 1d). Through analysis of the previously mapped mare units using the Chandrayaan-1 Moon Mineralogy Mapper (M3) data, Thaisen et al. suggested that the oldest mare unit Im was likely the remnant of the impact melt sheet, which was important to explore the geologic context of initial lunar crustal development and modification [12]. Pieters et al. found that there were several small exposures of three separate but distinctive rock types along the innermost Moscoviense Basin ring using M3 data and detected olivine, orthopyroxene, and Mg-rich spinel along the southwest sector of the peak-ring [13]. Bhatt et al. re-classified the previously mapped unit Iltm using Chandrayaan-1 visible-near infrared (VIS-NIR) data and named the northern part as unit Ivltm (Imbrian very low Ti and very low Fe) because of its lower titanium and the absolute model age [14]. The different understanding of the basaltic units also presents the difficulty in studying the basaltic volcanism by only using the spectral data.

This is mainly because the penetration depth of the used spectral data is rather low, only several microns below the lunar regolith [15–18]. In such depth, the regolith can easily be affected by the space weathering and the impact ejecta from nearby, or even far away regions [14,15]. The impact events from Titov crater (150.28°E, 28.55°N) within the Basin floor and abundant craters outside have clearly altered the surface compositions and topography, which is inevitable to affect the understanding of the basaltic units of Mare Moscoviense. How to mitigate such disadvantages and to better explore the regolith thermophysical features in situ is a critical problem in current lunar studies.
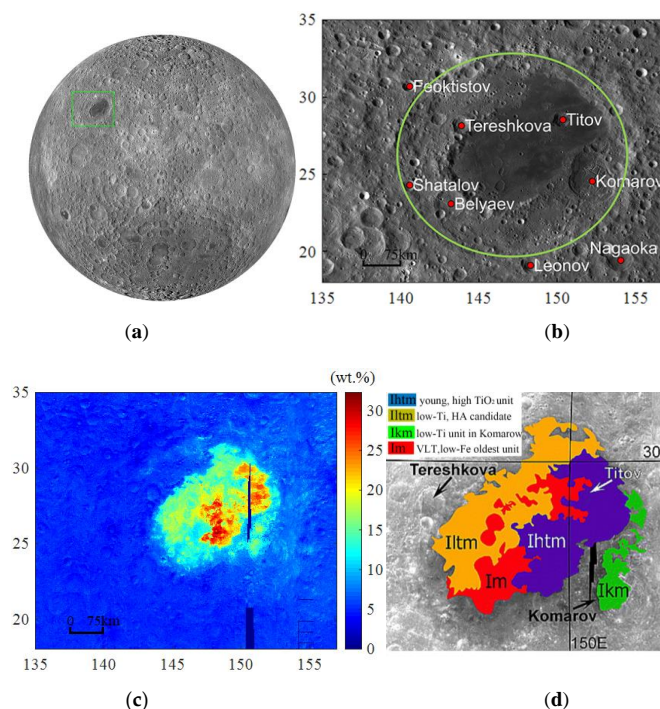
Figure 1. (**a**) Position of Mare Moscoviense (Green rectangle) on the lunar farside. (**b**) A mosaic of optical images from Lunar Reconnaissance Orbiter Camera (LROC), which was downloaded from https://astrogeology.usgs.gov/search/map/Moon/LRO/LROC_WAC; the green circle is an identified circle related to the rim of Mare Moscoviense. (**c**) Iron and titanium abundances (wt.%), which was estimated with the Lucey model [19] based on Clementine ultraviolet-visible (UV-VIS) data downloaded from https://astrogeology.usgs.gov/search/map/Moon/Clementine/UVVIS. (**d**) Geologic map [9] of Mare Moscoviense.

It is known that the observations in the microwave domain can eliminate well the aforementioned disadvantages [15–18]. For the first time, the Microwave Sounder (CELMS) onboard Chang'E-1/2 (CE-1/2) missions was used to measure the thermal emission of the lunar regolith in microwave domain. For the absence of the water on the Moon, the signal in microwave range can penetrate the regolith up to 10 to 20 times the wavelength [15,16]. The wavelength of the microwave used by the CELMS instrument is about 10 cm at 3.0 GHz, 3.85 cm at 7.8 GHz, 1.55 cm at 19.35 GHz, and 0.81 cm at 37 GHz. Correspondingly, the penetration is about 1 m–2 m at 3.0 GHz, 38.5 cm to 75 cm at 7.8 GHz, 15.5 cm to 31 cm at 19.35 GHz, and 8.1 cm to 16.2 cm at 37 GHz, which is decided by the FTA of the lunar regolith [15–18]. Moreover, the CELMS data has been proved to be sensitive to the substrate compositions and temperature [16–18,20,21]. Therefore, the CELMS data provides a potential chance to better understand the basaltic units in Mare Moscoviense. In this paper, the CELMS data from CE-2 satellite is used to evaluate the regolith thermophysical features of the mare basalts in Mare Moscoviense. In Section 2, the brightness temperature (T_B) and its influential factors are numerically studied with the radiative transfer simulation. The CELMS data processing is presented in Section 3. Section 4 briefly presents the T_B features of basaltic units at noon and at midnight, as well as the corresponding absorption features. Section 5 gives interpretations of the special findings in Moscoviense Basin indicated by the CELMS data, and Section 6 presents the conclusions.

2. Brightness Temperature of the Lunar Regolith

The T_B of the Moon and its characteristics were well investigated theoretically by a number of authors [22,23]. The orbital T_B measurements at different frequencies were proposed since the 1980s [24], with the expectation that they could lead to the knowledge of global lunar heat flow and average regolith thickness. This thermal information could provide a reliable estimation of substrate thermophysical features which are less contaminated by the ejecta in the uppermost layer [20,25,26].

To better understand the findings with the T_B and the T_B difference (dT_B) derived from the CE-2 CELMS data, the radiative transfer theory is used to model the thermal emission from the regolith. A commonly used regolith model is a two-layer model, which only takes into account the regolith and rock layers [20,24]. T_B of the lunar regolith has two components: T_{B1}, representing the radiation from the regolith layer, and T_{B2}, representing the radiation from the rock layer. T_{B1} also comprises upwelling, T_{1up}, and downwelling, T_{1dn}, radiations. The expression is expressed as follows:

$$T_B = T_{B1} + T_{B2} = T_{1up} + T_{1dn} + T_{2up}. \tag{1}$$

here,

$$dT_{1up} = \frac{1 - r_{p1}}{1 - L} k_{a1}(z) T(z) \sec \theta_1 e^{-\int_0^z k_{a1}(z') \sec \theta_1 dz'} dz, \tag{2a}$$

$$dT_{1dn} = \frac{(1 - r_{p1}) r_{p2}}{1 - L} k_{a1}(z) T(z) \sec \theta_1 e^{-(\int_z^d k_{a1}(z') \sec \theta_1 dz' + \int_0^d k_{a1}(z') \sec \theta_1 dz')} dz, \tag{2b}$$

$$dT_{2up} = \frac{(1 - r_{p1})(1 - r_{p2})}{1 - L} k_{a2}(z) T(z) \sec \theta_2 e^{-\int_d^z k_{a2}(z') \sec \theta_2 dz'} dz \cdot e^{-\int_0^d k_{a1}(z') \sec \theta_1 dz'} \tag{2c}$$

where d is the regolith layer thickness, θ_1 and θ_2 are the incidence angles of the regolith and the rock, respectively, $p = h$ or v, which corresponds to the horizontal and vertical polarizations, k_{a1} and k_{a2} are the absorption coefficients in the lunar regolith and rock layers, respectively, $T(z)$ is the temperature profile, r_{p1} and r_{p2} represent the effective reflectivity values of the free space-regolith and regolith-rock interfaces, respectively, and $1/(1-L)$ is the multi-reflection coefficient.

The dielectric constant is a decisive factor for the parameters including r_{p1}, r_{p2}, k_{a1}, and k_{a2}., which was obtained by Heiken et al. through assessing the relationship between the real part of the dielectric

constant ε', the loss tangent tanδ and the FTA value S (wt.%), based on the experimental study [27]. The relationship is expressed in the following:

$$\begin{cases} \varepsilon' = 1.919^{\rho}, \\ \tan\delta = 10^{0.038S+0.312\rho-3.260}, \end{cases} \tag{3}$$

where ρ is the density of the lunar regolith.

Then, the relationship between T_B and the thermophysical parameters of the lunar regolith can be constructed by integrating Equations (1) to (3) over the total thickness d.

The observation angle of the CELMS instrument is 0°, so that the polarization effect can be eliminated from the simulation. Moreover, Meng et al. proposed that the regolith thickness d plays a weak role on the T_B [28]. Thus, the regolith is assumed to be a 6-m-thick layer with a smooth surface. The temperature profile is calculated with the thermal conductivity model and the outmost depth temperature is assumed to be 252 K [23] as a constraint to solve the model. The hyperbolic model is used as the density profile ρ. The dielectric constant of the substrate rock is assumed to be 6.15 + i0.155 (dielectric constant of sample No.1555 from Apollo 15 mission). Meanwhile, the lunar surface temperature changes greatly with time of a day and the latitude position. Supposing the surface temperatures of 390, 300 (typical daytime temperature), and 200, 100 K (typical nighttime temperature), the change of T_B with FTA for the different surface temperatures can be simulated with Equations (1) to (3) (Figure 2).
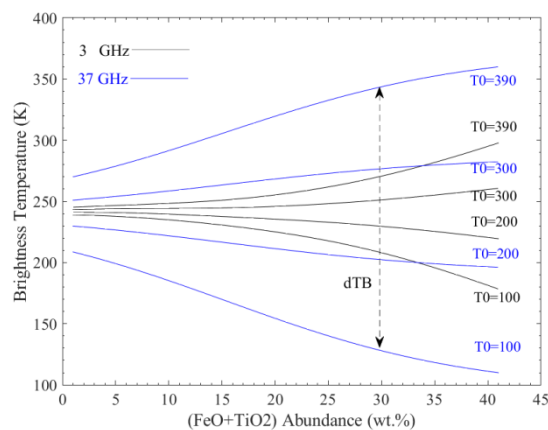
Figure 2. Change of simulated T_B with(FeO+TiO$_2$) abundance and surface temperature.

Figure 2 postulates a good description of the T_B performances over the lunar surface as the following three aspects.

Firstly, the daytime T_B is higher than the nighttime T_B. Moreover, the daytime T_B at high frequency is higher than that at low frequency, while the nighttime T_B at a high frequency is lower than that at a low frequency. This conclusion is fundamentally important to understand the distribution of the T_B over the lunar surface.

Secondly, with the FTA increase from 1 wt.% to 41 wt.%, the noon T_B monotonously increases about 90 K at 37 GHz and about 30 K at 3.0 GHz, while the midnight T_B monotonously decreases about 80 K at 37 GHz and about 27 K at 3.0 GHz. Thus, the T_B in the region with high FTA should be higher than that with low FTA at noon, but it should be lower than that with low FTA at night. This conclusion is important to understand the high T_B anomaly of the Basin floor.

Thirdly, the dT_B, defined as the difference of the same-channel T_B from noontime to midnight, has been proved to be directly related to the regolith thermophysical features within the corresponding microwave penetration depth. In theory, the dT_B is similar to the T_B change caused by variation of physical temperature. Interestingly, the dT_B is up to about 320 K at 37 GHz and about 100 K at 3.0 GHz (40 wt.% FTA), which is considerably higher than the T_B changes only brought by the FTA at

daytime or nighttime. Even if the FTA is about 1 wt.%, the dT_B is still up to 70 K at 37 GHz and 9 K at 3.0 GHz. Therefore, the dT_B is more sensitive to the FTA compared to the other regolith thermophysical parameters. This conclusion is important to understand the basaltic units identified by the CELMS data.

Moreover, besides the aforementioned regolith thermophysical parameters, the particle size of the regolith is also an essential parameter to affect the propagation of the microwave [22–24]. However, for the mean particle size is only about 77 μm, the wavelength of the microwave used by the CELMS instrument is far longer than the particle size. Additionally, when studying the T_B performances in highlands with even FTA distribution, Meng et al. proposed that the particle size of the lunar regolith has a little effect on T_B [29]. Thus, the effect of the regolith particle size is neglected in this study.

3. Methods and Data Processing

The study area includes the whole Mare Moscoviense and the nearby highlands.

3.1. CELMS Data

CE-2 satellite is the second Chinese lunar satellite and was successfully launched on 1 October 2010. CE-2 has carried seven payloads, one of which is the CELMS instrument, aiming to acquire brightness temperature (T_B) data of the Moon both at noon and at night.

The CELMS instrument operated at 3.0 GHz, 7.8 GHz, 19.35 GHz, and 37 GHz, and the corresponding bandwidths are over 100 MHz, 200 MHz, 500 MHz, and 500 MHz, respectively. Integration time of CELMS is 200 ms [21,30]. The observation angle is 0° and the temperature sensitivity is better than 0.5 K. The original spatial resolution is about 1° (about 30 km at the lunar equator) along the latitude, which is identical for the four channels. All data used was in 2C-level after system calibration and geometric correction, and it follows the format of Planetary Data System. As a single file, the 2C-level data contains a header and a table of measured data, which present the observation time, four-channel brightness temperatures, solar incidence and azimuth angles, selenographic latitude and longitude, orbit altitude, and data quality state. The CELMS data is available on request from http://moon.bao.ac.cn/searchOrder_pdsData.search.

A detailed description of the CELMS instrument and data was given by Wang et al. [26], Cai and Lan [30], and Zhu et al. [21].

3.2. T_B Maps Generation

From October of 2010 to May of 2011, the CELMS operated for near 5000 h cumulatively, and a total of 2394 tracks of swath CELMS data were collected. The observed data are enough to cover the Moon at least eight times.

In this paper, the study area is given as 18°N to 35°N in latitude and 135°E to 157°E in longitude, which includes the whole Mare Moscoviense and the nearby highlands. According to the range, the number of the selected original CELMS data is up to 29,454 points.

The CELMS data processing procedure is similar to that of the processing used in Mare Imbrium and Apollo Basin [17,18]. Firstly, the time angle, defined as the longitude difference between the observation point and the subsolar point, is used to attribute the selected data into 24 time spans. For the limitation of the observation time of the CE-2 satellite, only in the time spans from 13 to 14 o'clock and from 0 to 1 o'clock, the numbers of the CELMS data are present in enough quantity to cover the whole study area. Thereafter, the bilinear interpolation method is used to generate the T_B maps with a spatial resolution of 0.25° × 0.25°, about 7 km × 7 km in this region. Figure 3 is the generated T_B map in the time spans from 13 to 14 o'clock, which largely represents the microwave thermal emission (MTE) features of the lunar regolith at noontime. Figure 4 is the T_B map in the time spans from 0 to 1 o'clock, which represents the MTE features of the lunar regolith at midnight. The surface temperature at noontime is considerably higher, about 370 K, than that at midnight, about 71 K [27,31]. These time spans represent the two extreme phases of the MTE, which are appropriate to study the regolith thermophysical features of the basaltic units [17,18,32].
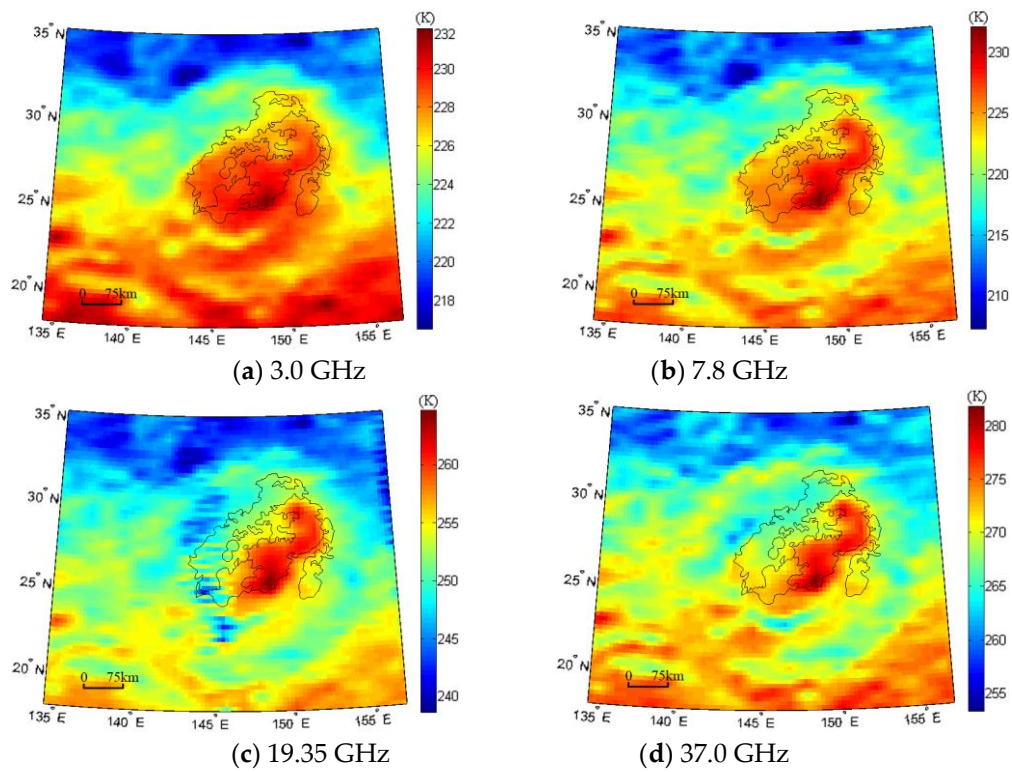
Figure 3. Noontime T_B maps of Mare Moscoviense at 3.0 GHz (**a**), 7.8 GHz (**b**), 19.35 GHz (**c**), and 37 GHz (**d**) (Lambert Conformal Conic projection). The black line indicates the geologic boundaries proposed by Kramer et al. [9].
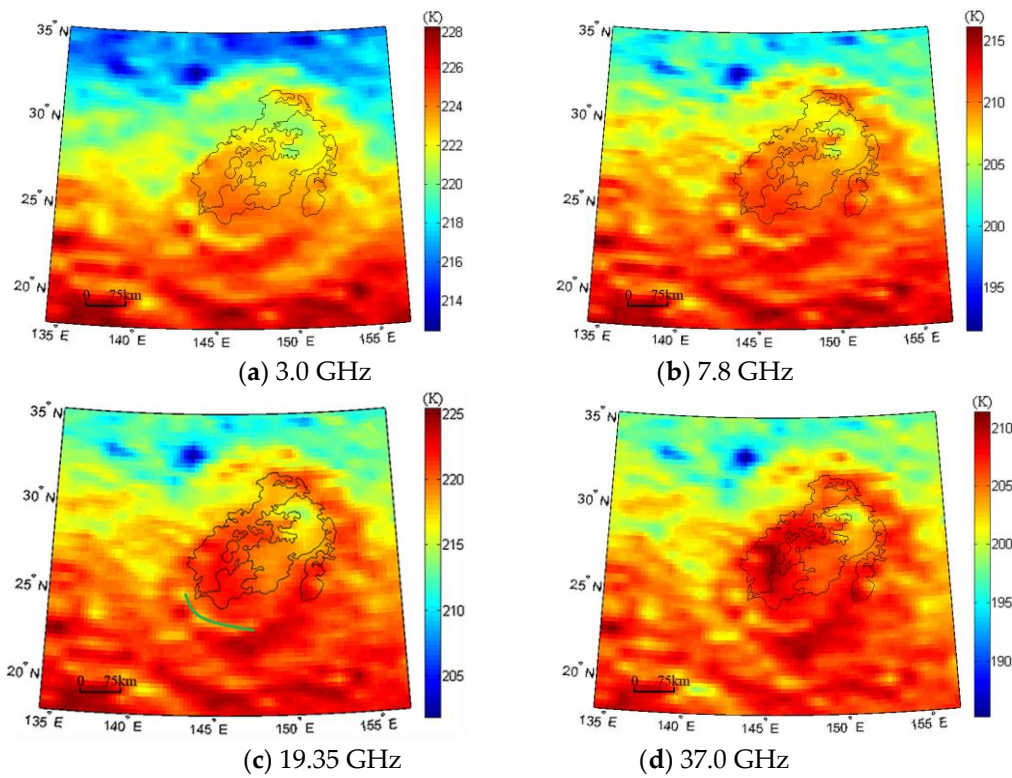
Figure 4. Nighttime T_B maps of Mare Moscoviense at 3.0 GHz (**a**), 7.8 GHz (**b**), 19.35 GHz (**c**), and 37 GHz (**d**) (Lambert Conformal Conic projection). The black line indicates the geologic boundaries proposed by Kramer et al. [9].

3.3. Image Analysis

The CELMS was the first orbital instrument to measure the MTE of the lunar regolith [33], which makes it hard to evaluate the spatial patterns of the generated T_B maps. Therefore, the geologic map proposed by Kramer et al. [9] is vectorized and overlain on the T_B maps to analyze the spatial patterns of T_B maps.

Figures 3 and 4 show, largely, a decent agreement between the geologic units and the T_B distributions. Especially in unit Ihtm in the eastern part of Mare Moscoviense, there exists an excellent coincidence between the unit boundary and the highest T_B at noon. Jin et al. [25], Wang et al. [26], Fang and Fa [16], and Meng et al. [20,34] all suggested that the region with higher FTA will have a relatively higher T_B at noon. Thus, the strong correlation between the high T_B at noon and high FTA in unit Ihtm directly indicates the rationality of the generated T_B maps.

Until recently, the T_B maps of the whole Moon were available by Wang et al. [26], Chan et al. [35], and Zheng et al. [36] using CE-1 CELMS data and Cai and Lan [30] and Zhu et al. [21] using CE-2 CELMS data. Our T_B maps agree well with the previous results, especially in Basin floor, which shows a relatively higher T_B than the nearby highlands both at noontime and midnight. This again implies the rationality of the generated T_B maps. In addition, our T_B maps firstly present a detailed view of the basaltic units in Mare Moscoviense compared to the previous results on a global scale.

However, there occur several belts with abnormally low T_B values in Figure 4c, indicating the problem of the data quality in this channel. Despite this setback, the T_B beyond the anomaly belts presents a good correlation with the T_B in other three channels. Therefore, the 19.35 GHz T_B at noon is only used as a reference in this study.

Theoretically, the surface slope also plays a significant role on the T_B [18,20,21,35–37], which may change the surface temperature and then indirectly alter the thermal emission of the lunar regolith. Correspondingly, the weakened T_B in the northern part of the Basin wall is just located in the slope opposite to the solar illumination as shown in green line in Figure 5, while the T_B in the southern part of the Basin rim is clearly enhanced. To better understand the influence of the surface topography, the elevation map from Lunar Reconnaissance Orbiter (LRO) lunar orbiter laser altimeter (LOLA) data is also introduced (Figure 6).
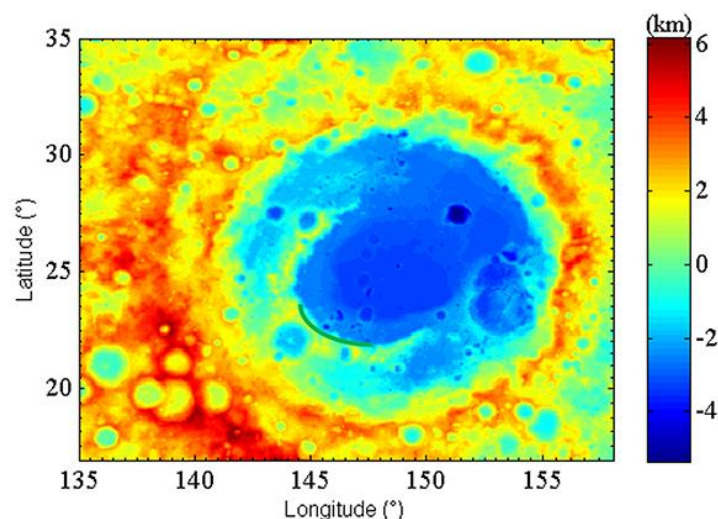
Figure 5. Elevation map of Moscoviense Basin. The green line is in the same place as in Figure 4c. The data is downloaded from https://pds-geosciences.wustl.edu/missions/lro/lola.htm.

However, Figure 5 indicates that, though the change in the elevation is about 10 km in Moscoviense Basin, regions seldom show the topography feature in the T_B maps. Even in the surrounding mountains and the considerably large craters such as Titov and Komarov, no special T_B distributions can be attributed to the slope. Moreover, in the following dT_B maps as shown in Figure 6, no surface

topography is reflected. Therefore, the T_B distributions are slightly affected by the surface topography, which is also neglected in the following discussion.
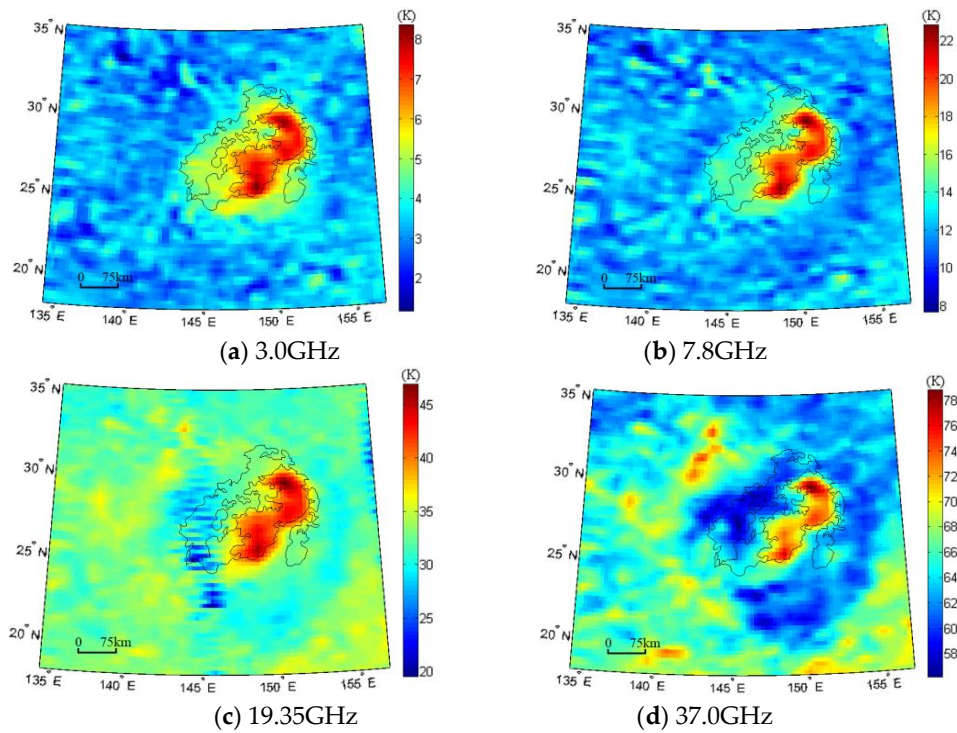
Figure 6. dT_B map of Mare Moscoviense at 3.0 GHz (**a**), 7.8 GHz (**b**), 19.35 GHz (**c**), and 37 GHz (**d**) (Lambert Conformal Conic projection). The black line indicates the geologic boundaries proposed by Kramer et al. [9].

Furthermore, the T_B distributions show a good corresponding with the basaltic units with high FTA, indicating potential geologic feasibility in understanding the basaltic units compared to the optical, thermal infrared data, and other sources of data.

3.4. Maximum Likelihood Classification

To better understand the basaltic units objectively, the classification method is preferred to comprehensively categorize the T_B into different geologic units. Among all the classification methods, the maximum likelihood classification (MLC) has a relatively higher precision [38,39], which is adopted in this study.

MLC is a classic probabilistic method based on the Bayes' principle. In this classification, a pixel is assigned to the class that has the highest probability (that is, the maximum likelihood). Mean vector and covariance metrics are the key component of MLC that can be retrieved from training data selected by the regions of interest (ROIs) file [38,39]. According to the maps by Morota et al. [11] and Bhatt et al. [14], six classes are interpreted, including the units Ihtm, Iltm north (unit Iltm1), Iltm south (unit Iltm2), Im, Ikm, and the highlands unit. The T_B data in Figures 3 and 4, and the following dT_B data in Figure 6, except that at 19.35 GHz, are used for our re-classification. That is, $\boldsymbol{T_B} = (T_{B1}, T_{B2}, T_{B3}, T_{B4}, T_{B5}, T_{B6}, T_{B7}, T_{B8}, T_{B9})$ is used for MLC classification. For each pixel $\boldsymbol{T_{Bs}} = (T_{B1,s}, T_{B2,s}, T_{B3,s}, T_{B4,s}, T_{B5,s}, T_{B6,s}, T_{B7,s}, T_{B8,s}, T_{B9,s})$, the MLC assumes that its distribution obeys the Gaussian distribution conditional on one specific class, $\{s|s = (i, j), 1 \leq i \leq m, 1 \leq j \leq n\}$ and $m \times n$ is the size of the image. Thus, the probability is expressed as:

$$P(\boldsymbol{T_{Bs}}|c_l) = \frac{1}{(2\pi)^3 \det|\Sigma_l|^{1/2}} \exp\left\{-\frac{1}{2}(\boldsymbol{T_{Bs}} - \mu_l)^T \Sigma_l^{-1}(\boldsymbol{T_{Bs}} - \mu_l)\right\}, \ 1 \leq l \leq 9 \qquad (4)$$

where $\theta_l = (\mu_l, \Sigma_l)$ is the mean and variance of Gaussian distribution for class c_l ($1 \leq l \leq 6$), and det $|\Sigma_l|$ is the corresponding determinant of Σ_l. According to this equation, the discriminant likelihood function of each class c_l for T_{Bs} is:

$$L\left(c_l, \theta_l, T_{Bs}\right) = P(c_l|T_{Bs}) = \frac{P(c_l)P(T_{Bs}|c_l)}{P(T_{Bs})}, \quad 1 \leq l \leq 9 \tag{5}$$

Because $\ln[P(T_{Bs})]$ is a constant for all the classes, the energy function is expressed as:

$$
\begin{aligned}
l(c_l, \theta_l, T_{Bs}) &= \ln[L(c_l, \theta_l, T_{Bs})] = -\ln[P(T_{Bs}|c_l)] - \ln[P(c_l)] \\
&= -3\ln(2\pi) - \tfrac{1}{2}\ln[\det|\Sigma_l|] + \tfrac{1}{2}(T_{Bs} - \mu_l)^T \Sigma_l^{-1}(T_{Bs} - \mu_l) - \ln[P(c_l)], \quad 1 \leq l \leq 9
\end{aligned}
\tag{6}
$$

where $P(c_l)$ is the priori probability. According to the MLC, the optimal class c_l^* of T_{Bs} should have the maximum $L(c_l, \theta_l, T_{Bs})$, i.e., the minimum $l(c_l, \theta_l, T_{Bs})$. That is:

$$
\begin{aligned}
c_l^* &= \underset{c_l}{arg\,max} L(c_l, \theta_l, T_{Bs}) = \underset{c_l}{arg\,min} l(c_l, \theta_l, T_{Bs}) \\
&= \underset{c_l}{arg\,min} - 0.5 * \ln[\det|\Sigma_l|] + 0.5 * (T_{Bs} - \mu_l)^T \Sigma_l^{-1}(T_{Bs} - \mu_l) - \ln[P(c_l)], \quad 1 \leq l \leq 9
\end{aligned}
\tag{7}
$$

The MLC method is used to re-understand the basaltic units in Section 5.1.

4. Results

Based on the overlap of the interpreted geologic boundary over the generated maps, a distinct perspective of the basaltic units compared to the visible image is presented in Figures 3 and 4.

4.1. Noontime T_B Features

Figure 3 is the T_B of Moscoviense Basin at noon. To better understand the thermophysical features of the mare, the maximum, minimum, average, and standard deviation (std.) of the T_B values in the four basaltic units interpreted by Kramer et al. [9] are presented in Table 1.

Table 1. Statistical values of the four mare units at noon.

Frequency (GHz)	Geologic Units	T_B (K)			
		Maximum	Minimum	Average	Standard Deviation
3.0	Ihtm	232.0	227.4	229.5	1.0
	Iltm	229.3	224.6	227.3	1.2
	Im	230.5	226.5	228.6	0.9
	Ikm	228.8	226.4	227.6	0.6
7.8	Ihtm	232.0	224.4	228.1	1.4
	Iltm	225.6	219.3	223.0	1.6
	Im	227.6	221.7	225.0	1.2
	Ikm	225.4	221.3	222.9	1.1
19.35	Ihtm	264.6	256.3	260.2	1.5
	Iltm	256.2	247.3	251.9	1.8
	Im	259.9	242.6	253.8	3.6
	Ikm	255.4	251.7	253.3	1.0
37	Ihtm	281.7	272.5	276.5	1.7
	Iltm	271.4	264.5	267.6	1.6
	Im	275.5	267.4	271.9	1.5
	Ikm	272.4	268.4	270.5	1.1

Figure 3 and Table 1 both indicate that unit Ihtm (the southern part of Mare Moscoviense) has the highest T_B at noon. Correspondingly, the FTA is highest in this unit. This correlation agrees well with the theoretical simulation [17,18,20], also indicating the rationality of the generated T_B maps.

In unit Iltm (the western and northern parts of Mare Moscoviense), the T_B performance is rather complex. Morota et al. [11] and Bhatt et al. [14] have mentioned the difference of the regolith components and the absolute ages between the southern and northern parts of this unit. Figure 3 shows that the T_B in the northern part is apparently lower than that in the southern part at the four-channel maps, while the boundary indicating the abrupt T_B changes is not clear between the two parts. Additionally, considering the decrease of the surface temperature with the latitude increase, about 20 K from 18°N to 35°N, this T_B performance should not be attributed completely to the difference in the regolith thermophysical features.

Moreover, the T_B in the southern part of unit Iltm is similar to that in unit Im (the southwestern part of Mare Moscoviense), while the T_B in the northern part is clearly higher than the nearby highlands at 3.0 GHz but similar to the nearby highlands in the other three channels. Additionally, the area of the region with relatively lower T_B becomes larger with the increasing frequency. Combined with the penetrative features of the microwave signals [15,20], this implies the rapid change of the regolith thermophysical features in vertical direction because of the very different T_B performances at the four channels.

Unit Im presents a special T_B performance. Figure 3 postulates a relatively higher T_B compared to unit Iltm. Table 1 validates this finding by maximum and average values. However, Figure 1c illustrates that the FTA in this unit is lower than unit Iltm, which is not supported by the theoretical simulation as shown in Figure 2. What brings such enhanced T_B performance should be further studied.

Because the area of unit Ikm (mainly within Komarov crater) is rather small compared to the original spatial resolution of the CELMS data, about 30 km along the latitude, the MTE features of unit Ikm are hard to understand in Figure 3. Though there exists the T_B variation within the unit, the difference between the unit and its vicinity is not clear.

Interestingly, there exists a very high T_B region near (148.5°E, 25°N) in the southern part of unit Ihtm, but there is not any terrain or FTA distribution that is consistent with this anomaly. This abnormal T_B will be further discussed in Section 5.2.

Furthermore, though there occurs an about 20 K T_B variation with the latitude, the T_B in Basin floor is still higher than the highlands, especially in unit Ihtm. This means that the regolith thermophysical parameters play a relatively more important role on the observed CELMS data.

4.2. Nighttime T_B Features

Compared to Figure 3, Figure 4 provides an alternate view about the MTE features of the basaltic units. Table 2 also gives the statistical values of the T_B in the four basaltic units.

Table 2. Statistical values of the four mare units at midnight.

Frequency (GHz)	Geologic Units	T_B (K)			
		Maximum	Minimum	Average	Standard Deviation
3.0	Ihtm	224.0	220.3	222.1	1.0
	Iltm	224.3	220.1	222.3	1.1
	Im	224.8	220.3	223.5	1.1
	Ikm	224.3	222.4	223.3	0.6
7.8	Ihtm	211.5	205.3	208.7	1.5
	Iltm	212.6	205.0	208.8	1.5
	Im	212.3	204.7	210.3	1.6
	Ikm	212.1	208.0	210.0	1.0
19.35	Ihtm	221.6	214.0	218.5	1.6
	Iltm	222.7	216.4	219.8	1.5
	Im	222.5	216.1	220.6	1.5
	Ikm	222.7	218.6	220.4	1.0
37	Ihtm	207.9	199.0	204.8	1.9
	Iltm	211.3	202.2	207.2	2.1
	Im	210.2	201.8	207.9	1.7
	Ikm	208.6	202.7	205.4	1.5

Figure 4 and Table 2 both indicate that the lowest T_B occurs in unit Ihtm and the highest T_B occurs in unit Im. Combined with the FTA in units Ihtm, Iltm, and Im, this nighttime T_B performance is rational according to the theoretical simulation and the findings with the CELMS data [34], again justifying the use of the generated T_B maps.

In unit Iltm, similar complex phenomena again exist. The T_B in the northern part is largely lower than that in the southern part at the four-channel maps. Furthermore, the area of the region with relatively lower T_B is decreasing with the increasing frequencies. Interestingly, at 37 GHz, the highest T_B of Moscoviense Basin occurs in the southern part of Iltm unit. This verifies the complexity of the regolith thermophysical features in this unit as demonstrated by the T_B performances at noon.

Theoretically, the T_B performances at noon will be inversely corresponding to those at midnight [20,26,34]. However, the difference among the average T_B values of the four units is rather weak, no more than 3 K. This is much less than that at noon, up to 10 K. The reason for the low T_B difference should be further studied to better understand the substrate regolith thermophysical features of the Msocoviense Basin.

What was found to be quite puzzling is the T_B performance within the Basin floor. Here, since the FTA is higher than the nearby highlands, the T_B during daytime is higher than the nearby highlands. However, the T_B at nighttime is still higher than the highlands along the same latitude, which is contrary to the theoretical simulation. The causes of the high T_B anomaly should be further discussed in the following study.

4.3. dT_B Features

Though Figures 3 and 4 are largely adequate at indicating the thermophysical features of the mare basalts in Moscoviense Basin, the change of the T_B with latitude limits our understanding of the distribution features of the basaltic units.

Considering that the great change of the lunar regolith temperature only occurs in the upper 15 cm [26,37], Meng et al. [17,18,20] suggested that the dT_B should be directly related to the regolith thermophysical features within the corresponding microwave penetration depth based on the theoretical simulation. Therefore, the dT_B map is also generated in this study (Figure 6). Table 3 gives the statistical values of the dT_B in the four basaltic units.

Table 3. Statistical values of the four mare units.

Frequency (GHz)	Geologic Units	dT_B (K)			
		Maximum	Minimum	Average	Standard Deviation
3.0	Ihtm	8.4	5.7	6.9	0.5
	Iltm	6.5	3.8	5.0	0.5
	Im	7.1	3.4	5.1	0.7
	Ikm	5.0	3.5	4.3	0.4
7.8	Ihtm	22.8	16.0	19.4	1.4
	Iltm	18.2	12.2	14.2	0.8
	Im	19.6	12.0	14.7	1.4
	Ikm	14.0	11.9	12.9	0.6
19.35	Ihtm	46.9	37.3	41.7	1.9
	Iltm	38.8	25.3	32.1	2.3
	Im	42.2	21.8	33.2	4.1
	Ikm	34.3	32.2	33.0	0.5
37	Ihtm	78.8	66.7	71.7	2.4
	Iltm	68.1	56.1	60.4	2.0
	Im	72.1	60.2	64.9	2.1
	Ikm	66.7	61.5	62.5	1.1

Figure 6 shows an interesting dT_B performance, which can be expressed as follows.

Firstly, comparing the three basaltic units in the Basin floor, the highest dT_B exists in unit Ihtm at all channels, which is about 2 K at 3.0 GHz, 5 K at 7.8 GHz, and 7 K at 37 GHz higher than that in the second highest region, unit Im.

Interestingly, the dT_B difference between unit Im and unit Iltm is not clear at low frequencies. The dT_B in unit Iltm is only about 0.1 K at 3.0 GHz and 0.5 K at 7.8 GHz higher than that in unit Iltm, which means that the substrate materials in depth layer of the two units are likely similar. However, at 37 GHz, the dT_B in unit Im is up to 4.5 K higher than that in unit Iltm, indicating that the difference of the materials in the two units only occur in the shallow layer.

Comparatively, unit Ikm has the lowest dT_B at 3.0 and 7.8 GHz, while the dT_B in this unit is approximately 2 K higher than that in unit Iltm at 37 GHz. Moreover, the regions with high dT_B values do not coincide with the boundary of unit Ikm. Such dT_B performance is hard to interpret, which also deserves to be further studied.

Secondly, in highlands, Figure 6 indicates a new view on the regolith thermophysical features. The dT_B variation in highlands beyond Mare Moscoviense is no more than 2 K at 3.0 GHz and 4 K at 7.8 GHz. Moreover, the aforementioned dT_B variations should be attributed in part to the topography, as the change of the surface elevation is approximately 10 km [27]. The approximate dT_B values imply the similar lunar regolith parameters in highlands surrounding Mare Moscoviense, which at least indicates the homogeneity of the regolith thermophysical parameters in the depth layer of the highlands. This also indicates that the CELMS data is a good candidate to evaluate the basaltic units in Moscoviense Basin.

However, at 37 GHz, the dT_B in the eastern part is about 6 K lower than that in the western part. Interestingly, the area with rather low dT_B originates from the boundary between units Iltm and Im, extending along the northeast direction, and spreading toward the southwest direction along the southern boundary of unit Ihtm. The rather low dT_B regions clearly terminate in the south part of the Basin. Especially in the region near (145°E, 20°N), the boundary between the low dT_B region and the high dT_B region is fairly clear, although they both belong to the highland regions. Additionally, although the data quality is not good at 19.35 GHz, the regions with relatively lower dT_B largely coincide with that at 37 GHz. Such a coincidence verifies that this is an actual difference in the regolith thermophysical features between the eastern and western highlands of the Moscoviense Basin. Combined with the previous analysis, the depth of the special materials is more than 16.2 cm but less than 76.9 cm.

The surface topography (Figures 1b and 5), the FTA map (Figure 1c), and even the rock abundance from Bandfield et al. [40] could not be responsible for the abnormally low dT_B, indicating that this is a special finding only revealed by the CELMS data. What brought about the low dT_B here leaves much room for further studies, which may consequently bring about an improved understanding of the formation of the highlands.

Thirdly, in general, the FTA in the Basin floor is higher than the nearby highlands. Theoretically, the dT_B in the Basin floor should also be higher than the nearby highlands. The dT_B performances at 3.0 and 7.8 GHz are good evidence to support this theoretical simulation. Additionally, at 37 GHz, the dT_B performance in units Ihtm and Im agrees well with the theoretical simulation. However, the dT_B in unit Iltm is not only lower than in unit Im, but also lower than in the western highlands, and it is just as low as in the eastern highlands. This is also a new finding revealed by the CELMS data, which will test our understanding on the basaltic volcanism in Mare Moscoviense.

Additionally, there exists a significant T_B change in maps near 26°N both at noon and midnight. However, no surface topography or composition distribution can be responsible for the T_B change. Particularly, the dT_B performances do not support this T_B change near 26°N, which indicate the similar values in the highlands surrounding Mare Moscovinse at 3.0 and 7.8 GHz maps. Thus, combined with the numerical simulation, this T_B change is likely brought by the great change of the surface temperature with latitude, which is about 20 K from 18°N to 35°N.

This also postulates that the surface temperature has a weak effect on the dT_B, which is very important to further explore the lunar surface with the CELMS data.

5. Discussion

The T_B and dT_B features indicate several special findings of Mare Moscoviense.

5.1. A New View of Basaltic Units

The understanding of the basaltic volcanism is mainly depended on the identification of the basaltic units. Until now, the most important dependence to divide the Basin floor into units is the spectral data and the inferred FTA with Clementine UV-VIS data and the Chandyayaan Moon Mineralogy Mapper data here [9,11,14]. However, the penetration depth of the spectral data is limited at the uppermost layer of the lunar regolith, which is easily impacted by the space weathering and ejecta from other regions [15,16,27]. Therefore, the previous interpretation of the basaltic units could be re-evaluated using the microwave data with better penetration capability.

In Mare Moscoviense, the identification of the basaltic units is mainly based on the Clementine UV-VIS data [9], Selene Terrain Camera data [11], and Chandrayaan-1 M3 data [14]. However, the geologic interpretations do not entirely agree with each other. Especially to the unit Iltm, Bhatt et al. [14] re-classified it as unit Ivltm (Imbrian very low Ti and very low Fe) in the northern part and kept unit Iltm in the western part, where the iron and titanium contents in unit Ivltm is 2–4 wt.% lower than unit Iltm.

Interestingly, the T_B performances show that only unit Ihtm is largely consistent with the spectral interpretation [9]. The difference between the southern and northern parts of unit Iltm is not clear in T_B maps. To better understand the basaltic volcanism objectively, the MLC method mentioned in Section 3.4 is preferred to comprehensively categorize the T_B into different geologic units.

Here, the ArcGIS software (version 10.2) is used to select the ROIs for every geologic unit, which are shown in Figure 7a. The training samples are used to estimate the mean vectors and covariance matrixes for the MLC classifier. These two parameters determine the properties of the multivariate normal models. Thereafter, the trained classifier was used to classify every pixel in the image into one of the desired classes. In order to reduce poor classification due to small probabilities, the predetermined threshold is set to 5% of the average measurements, and the total number of iterations is set to 1000. Once the training process terminates, the maximum likelihood classifier will rapidly identify the corresponding geologic unit for any given set of input parameters, T_B.

(a)   **(b)**
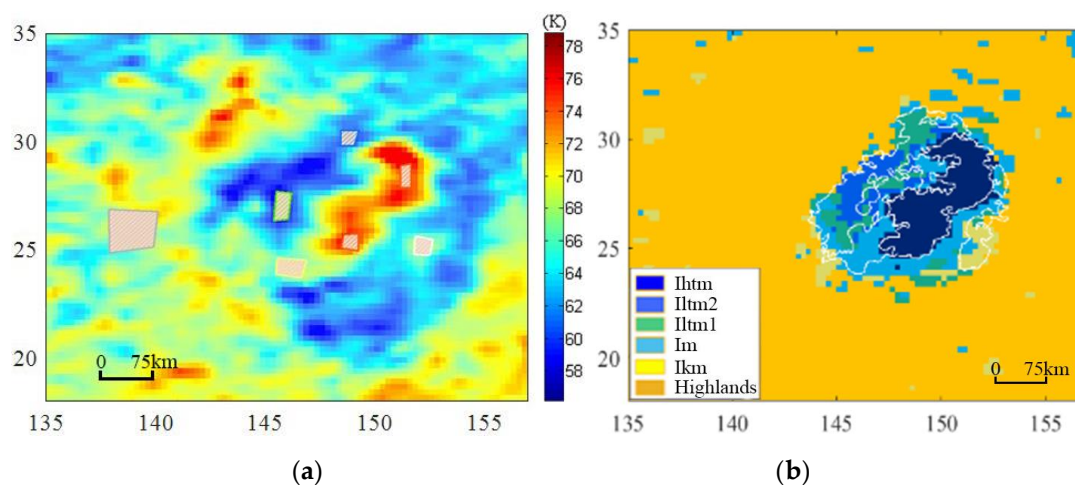
Figure 7. (**a**) The selected regions of interest (ROIs) for the classification. (**b**) The classification results related to the basaltic units overlaid by Kramer's result [9].

Through this method, the basaltic units and the highlands were interpreted as shown in Figure 7b. To better understand the new geologic map, the geologic map by Kramer et al. [9] was also vectorized and overlaid on the new map as shown in Figure 7b.

Figure 7b again indicates an excellent coincidence in unit Ihtm and highlands. This not only validates the rationality of the generated geologic map, but also verifies the reliability of the used CELMS data. However, there were also multiple patches indicated as mare units in the highlands. This is probably brought by the uncertainty of the MLC method, which is inevitable to misclassify few pixels with the remote sensing methods. Interestingly, when checking Figures 3–6 in these regions, we mentioned that the T_B and dT_B performances are abnormal compared to their vicinities. Particularly, the T_B and dT_B performances are abnormal in the crater near (153°E, 20°N), which is classified as unit Ikm; while T_B performances are normal in the nearby crater at (151°E, 20°N), which is classified as unit highlands. This means the difference of the two craters in volumetric regolith thermophysical features. This also hints the significance of the CELMS data in studying the deposits of the lunar surface.

In most cases, the unit boundary is smoother than that interpreted by Kramer et al. [9]. This results from the low spatial resolution of the CELMS data, about 7 km in this study, which will not be considered in the following discussions.

Compared to the previous results, the differences mainly occur in three aspects.

Firstly, unit Iltm does not agree with the western and northern separations by Bhatt et al. [14]. Figure 7b shows that unit Iltm2 is largely enclosed by Iltm1 unit. However, between units Iltm1 and Ihtm, there again occurs unit Iltm2. This phenomenon implies that the difference between units Iltm1 and Iltm2 are likely in the uppermost layer of the lunar regolith as indicated by the spectral data, but not in volume. Interestingly, Figure 6 indicates a similar dT_B performance as unit Im at 3.0 and 7.8 GHz, but a different performance at 37 GHz. Considering the probing penetration of the microwave is about 10 to 20 times the used wavelength [15], this phenomenon implies that the regolith properties in the shallow layer are different from those in depth. The FTA in mare basalts is relatively high compared to the highlands; this depth is more than 8.1 cm indicated by the 37 GHz map, but less than 38.5 cm indicated by the 7.8 GHz map. Thus, the aforementioned phenomena indicate that unit Iltm should be covered by a shallow layer of special material, which would then produce a rather low dT_B. That is, the difference between units Iltm1 and Iltm2 results from the ejecta overlay, but not from the mare basalts in different periods.

Additionally, a swirl occurs in this unit, which is often interpreted as albedo anomalies due to their immensely brighter, sinuous textures, and high immaturity [41]. The surge of magnetic fields in the swirl regions almost has no relation to topographical deformations [41]. Thus, this magnetic anomaly and the composition with spectral data may give some meaningful clues to improve understanding the very low dT_B and even the basaltic volcanism of the lunar farside, which should be further studied with more sources of data in future.

Secondly, the distribution of unit Im is much more extensive than that interpreted by Kramer et al. [9]. Unit Im is represented by the second highest T_B at noon, highest T_B at midnight, and the second highest dT_B. In the new geologic map, the area of unit Im extends in southwest direction, occupying the southwestern part of unit Iltm, and in northeast direction, forming a long belt in the southeast part of unit Ihtm. This is because, although the FTA in the extended regions is lower than the basaltic units, it is still higher than the nearby highlands. Correspondingly, the T_B performances are similar to that of unit Im.

Notably, the area of this unit near Titov crater is much less than before, part of which is identified as unit Ihtm. This again validates that such regions are covered by the impact ejecta with low FTA.

Thirdly, Figure 7b gives a good definition about unit Ikm. Though it is always attributed to unit Iltm [11,14], it is actually an independent unit in T_B performances. Compared to the geologic map by Kramer et al. [9], unit Ikm is limited in the western part of Komarov crater, while the northern part of the unit beyond Komarov crater is reclassified as unit Im. On the other hand, unit Ikm occurs

in the southwest part next to unit Im and the highland regions far from Mare region, indicating the complexity of the regolith thermophysical features in this unit.

Generally, the CELMS data provides a new view about the basaltic units in Mare Moscoviense compared to the Clementine UV-VIS results and the Chandrayaan-1 M3 results. Especially, the changes of the T_B and dT_B with the frequency bring some essential information about the substrate deposits. This is of special importance to promote the applications of the CELMS data in understanding the basaltic volcanism of the Moon.

5.2. Warm T_B Anomaly

Jin et al. [25], Wang et al. [26], and Meng et al. [34] proposed that the regions with high FTA will postulate high T_B at daytime, low T_B at nighttime, and a high dT_B as indicated by the simulation results in Section 2. Combined with Figures 1c and 3, Figure 4, and Figure 6, the T_B performances within Moscoviense Basin obviously support the conclusion. Here, the FTA of unit Ihtm is much higher than that in unit Iltm at noon, while it is apparently lower than unit Iltm at night, especially at 37 GHz. Again, the highest dT_B values in unit Ihtm clearly verify the conclusion.

Additionally, two phenomena should be mentioned.

Firstly, the FTA in the highlands beyond the Moscoviense Basin is much lower than that in highlands (Figure 1c). The T_B at noon and dT_B performances are corresponding to their FTA performances. These performances agree with the theoretical conclusion.

However, at midnight, the T_B in the Basin floor is still much higher than that in the highlands along the same latitude with lower FTA. This is totally opposite the aforementioned conclusion, hinting a warm T_B anomaly existed in the Basin floor. However, what brought about this warm T_B anomaly?

Interestingly, a similar phenomenon also occurs in the Orientale Basin. Combined with the theoretical simulation, Meng et al. [20] thought that there were three possible explanations to the abnormally high T_B at night, including the FTA, the surface slope, and the given substrate temperature. Additionally, Bandfield et al. [41] thought the rock abundance (RA) would bring about the hot T_B anomaly of the lunar surface in the thermal infrared domain. That is, in previous studies, the T_B anomaly is attributed to four regolith thermophysical features, including the FTA, surface slope, RA, and the substrate temperature.

The first parameter, the FTA of the lunar regolith, can be eliminated, because it gives an opposite result to interpret the warm T_B anomaly in the Moscoviense Basin.

The second parameter, surface slope, can also be neglected. As we know, the elevation change is more than 10 km from the Basin center to nearby highland, while there are no special T_B variations in Figure 3, Figure 4, and Figure 6 related to the Basin range, indicating the weak influence of the topography in macro-scale on the T_B performances. Additionally, what we found in Hertzsprung Basin also supports the conclusion [29]. That is, the influence of the surface slope on the warm T_B anomaly is rather weak and can, therefore, also be neglected.

For the third parameter, Chan et al. [35], Zheng et al. [36], and Meng et al. [29,42] suggested that the regions with higher RA will introduce the lower T_B at night. For the dielectric constants of the regolith with rocks will be enhanced, thus, the penetration depth of the microwave is reduced and the warm medium in depth cannot be sensed by the CELMS instrument as mentioned in Section 2. Moreover, according to the simulation results with the theoretical model, Gong and Jin [43] also proposed that the higher RA will bring about the lower T_B at night, which is also opposite to the observations in this study. Thus, this parameter can be omitted, too.

Therefore, the only leftover influential parameter is the substrate temperature. Until now, there were only two measured substrate temperatures at Apollo 15 and 17 sites, 250 K and 252 K, respectively [27]. The two values are always used as the substrate temperature when studying the MTE features over the whole lunar surface [20,25,26]. However, if the other parameters are omitted, only the higher substrate can be responsible for the higher T_B at night. A similar conclusion can

also be obtained in Mare Orientale and Crisium using the CELMS data [20,44]. That is, the substrate temperature of the lunar regolith in Moscoviense Basin is likely much higher than what we know.

The second phenomenon is that the FTA derived from the optical data is higher in unit Iltm than that in unit Im [9,12,14]. Thus, according to the theoretical simulation, the T_B in unit Iltm should be higher than that in unit Im. However, the T_B performances in the two units are just opposite to the theoretical simulation, as the observed T_B in unit Iltm is lower than that in unit Im at noon.

The above two phenomena together develop a new view on the temperature in the substrate within Mare Moscoviense, that is, the substrate temperature should be higher than the Apollo measurements and the relatively higher substrate temperature should occur exclusively in unit Im. Moreover, the T_B in unit Im is only 1.3 K higher than that in unit Iltm, indicating that the substrate temperature is about 3 K or less than the mentioned supposed depth temperature used in the numerical simulation in Section 2.

This is a new understanding about the distribution of the substrate temperatures in the shallow layer of the lunar surface. It is essential to study the thermal evolution of the Moon, which can be further studied with the experiment and, possibly, the in-situ observations.

5.3. Revealed Special Terrains

Figures 3, 4 and 6 show that the T_B performance in the southern part of unit Ihtm (marked Region A) is much different from that in the northern part (marked Region B) (Figure 8). Combined with Figures 1c and 3–6, a special volcanic process is expressed in unit Ihtm.
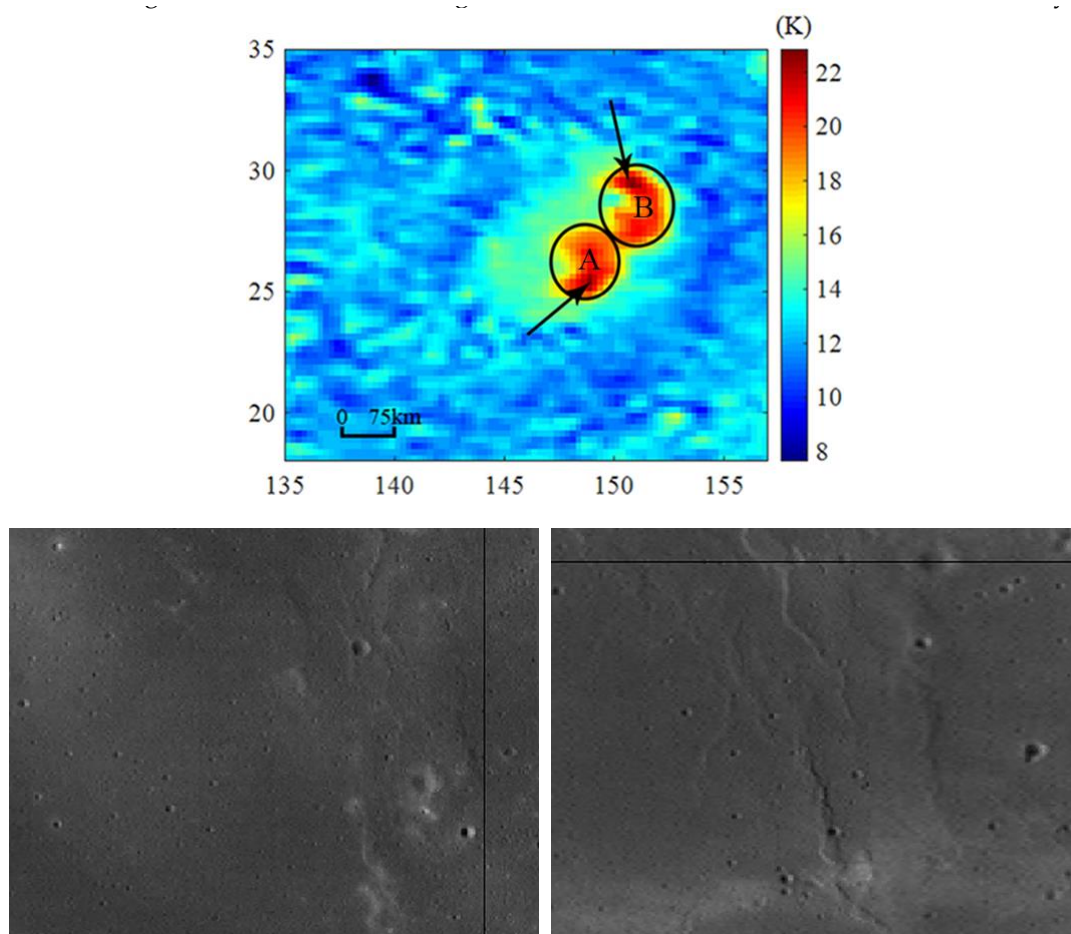
Figure 8. Two potential volcanic features outlined in dT_B map at 7.8 GHz (up) and the wide angle camera (WAC) images of Region A (bottom, left) and Region B (bottom, left), whose sizes are about 24 km × 23 km.

Firstly, Figure 1c indicates that, though the FTA in Region A is similar to that in Region B, the value in Region A is about 3 wt.% higher than that in Region B.

Secondly, Figure 3 indicates that the T_B in Region A is similar in amount to that in Region B at noon, while Figure 4 indicates a higher T_B in Region A compared to Region B at night.

Thirdly, Figure 6 illustrates that, at the four channels, Region A is not continuous with Region B, though they have the similar dT_B performances. Additionally, the regions with relatively higher dT_B are largely in the north-south direction, and the areas are decreased from the central part to the boundaries.

Therefore, Region A and Region B should be two isolated volcanic structures though they belong to one basaltic unit.

Moreover, the shape of the two regions is interesting, which indicates the inverse "C" pattern. Such patterns with similarly high FTA are widely identified in Marius Hills plateau and even on Earth, which is interpreted as the volcanic construct [12,45]. That is, Region A and Region B are most likely two independent volcanic features, probably the volcanic constructs.

Moreover, seeking for the volcanic origins is difficult on the lunar surface for the space weathering and the contamination of the impact crater ejecta [45,46]. Here, as mentioned in Section 3, they both have one small patch with highest dT_B in the four channels in Regions A and B. Considering the basalts with higher FTA are formed in the late volcanism [46], unit Ihtm has been identified as the late-stage lava basalt and the latest basalts should exist in the two small patches as indicated by the arrows in Figure 8 (up). Thus, the small patches with the highest dT_B in Region A and Region B are likely the locations of the fissures of the volcanic activity that led to the filling of Moscoviense Basin. Therefore, there likely exist two volcanic features in Moscoviense Basin. The diameters of the two volcanic features are about 60 km, which is much larger than the discovered volcanic constructs in most other regions of the lunar surface [47,48], therefore, hinting at the great strength of the volcanic sources in the Basin. This conclusion may in part be supported by the discovered thinnest crust of the entire Moon beneath Mare Moscoviense [5,6], for the eruption of the mare basalts in such depth may be easier than that in the regions with thick crust. If so, such huge volcanic features bring a special understanding about the basaltic volcanism over the lunar farside, which directly reveals the potential volcanic features beyond the optical data for the first time. This is of essential significance to re-understand the basaltic volcanism on the Moon with the CELMS data.

Additionally, the area of the patch with highest dT_B in Region A becomes smaller with increasing frequency. Moreover, in the 37 GHz map, the results are unclear. This means that the basaltic origin was disturbed in the shallow layer, which is also the reason that they are not observed by the spectral data. Furthermore, we checked the WAC image of Regions A and B as presented in Figure 8 (bottom), and multiple wrinkle ridges are found. We know little about the relationship between the wrinkle ridges and the basaltic volcanism, but the strong correlation between the wrinkle ridges and the high dT_B anomalies again validates the advantages of the CELMS data in the lunar volcanism study.

One more thing should be mentioned is the presence of floor-fractured craters in Moscoviense Basin. In particular, Komarov crater has extensive fractures and a massively bulging anomaly beneath the floor, indicating the ever-existed strong volcanic activities. Interestingly, the T_B in the crater floor is slightly higher in the southwestern part of unit Ikm than its vicinity both at noon and at night. Again, there exists a slightly high dT_B anomaly in the central part of the crater at 19.35 and 37 GHz maps, which can support the aforementioned correlation to certain extend. However, considered that the diameter of Komarov crater is only about 85 km and that the spatial resolution of the used CELMS data is about 30 km, it is difficult to further discuss the dT_B anomaly in the crater. Moreover, the weak dT_B anomaly may probably attribute in part to the difference in the formation mechanism of wrinkle ridge and floor fracture. More passive microwave observations are indispensable to improve studying the relationship between the wrinkle ridges and the high dT_B anomalies.

5.4. Homogeneity of Lunar Highlands

Pieters [49] and Tompkins and Pieters [50] proposed the idea that the lunar highlands crust below the surface is compositionally diverse by investigating the mineralogy of the central peaks. Wu et al. [51] studied the elemental abundances of the topmost surface of the lunar highlands with CE Interference Imaging Spectrometer (IIM) data, and concluded that the lunar highlands crust is relatively uniform on the quadrant scale, but inhomogeneous on the global scale. However, attention is seldom paid to the materials in the local highlands.

Until now, the regolith parameters in Moscoviense Basin have been widely studied with the Clementine UV-VIS data and Chandrayaan-1 M3 data [8], but no reports are related to the highlands materials surrounding the Basin floor. The dT_B has proved to be directly related to the regolith thermophysical features within the corresponding microwave penetration depth [17,18,20]. Thus, the four-channel dT_B maps in Figure 6 presents a new view of the homogeneity of the lunar highlands.

Figure 6 shows that the total dT_B variations are less than 4 K at 3.0 GHz and about 6 K at 7.8 GHz in the highlands regions surrounding the Moscoviense Basin. If the abnormally high and low dT_B values are excluded, the corresponding variations are only about 2 and 4 K, respectively. In previous studies, the temperature change as a result of solar illumination was reported to be up to 300 K from noon to midnight [27]. Such small dT_B variations in highlands regions directly indicate the similar regolith thermophysical features, indicating that lunar regolith is homogeneous in the highlands surrounding Mare Moscoviense at least in microwave domain.

However, at 19.35 and 37 GHz, the dT_B in the east highlands is about 6 K lower than that in the west highlands, which clearly suggests that the materials are not identical. The low dT_B region originates from the boundary between units Iltm and Im, extends along the northeast direction, and continues towards the southwest direction along the southern boundary of unit Ihtm, which is outlined in Figure 9. Moreover, low dTB appears as well in the northwest corner of the image. The dT_B values there are quite similar to those included in the outlined anomaly in the highlands on the southeast–north sectors of the Basin, which should be similar to the outlined anomaly, too. Thus, what are the causes for the low dT_B anomaly?
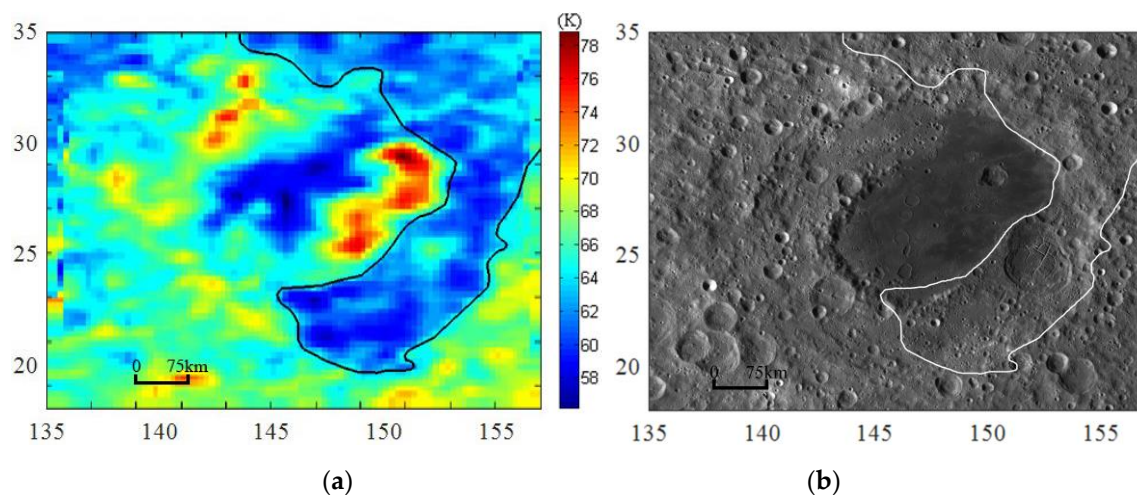
Figure 9. Low dT_B anomaly outlined in dT_B map at 37 GHz (**a**) and expressed in WAC image (**b**).

Though Kramer et al. [8], Morota et al. [11], Thaisen et al. [12], Pieters et al. [13], and Bhatt et al. [14] studied the compositions in Moscoviense Basin, no special material was mentioned in the surrounding highlands. This implies that the material is likely not identified by the optical data.

Interestingly, in geography, the low dT_B anomaly largely occurs in the eastern part of a ring structure as indicated by the green circle in Figure 1b. This is one of the rings related to the formation of Moscoviense Basin, meaning that the special material should be related to the excavation process

during the formation of the Basin [52]. Moreover, the special material is largely within the second ring next to the innermost ring, which hints that it should be ejected from the late stage impact forming the Basin floor. Considering Mare Moscoviense has the thinnest crust on the entire Moon [5–7], the special material should be excavated from the lower crust.

However, since the microwave has no ability to identify the components of the lunar regolith, the special material is still unknown. Meaningfully, Meng et al. [18,43,53] found that the low dT_B anomaly also occurs in the peak ring of Apollo and Schrödinger Basins and in the place surrounding Copernicus crater, indicating that the extensive occurrence of the low dT_B anomaly over the lunar surface. Moreover, the dT_B in unit Iltm and its north vicinity also indicates the rather low values, which is even lower than the east highlands. The relationship between this low dT_B anomaly and the east highlands is still not clear. Optimistically, after checking the T_B performances in Von Kármán crater, the low noontime and nighttime T_B anomalies clearly exist in the central part of the crater floor [54]. The on-going CE-4 mission is counted upon to bring some useful information to better understand the formation mechanism of the low dT_B anomaly and its geologic representations.

6. Conclusions

In this paper, the CE-2 CELMS data was systematically processed to study the MTE features of Mare Moscoviense. The T_B and dT_B performances present some interesting information about Moscoviense Basin and the surrounding highlands.

Firstly, according to the T_B and dT_B performances, the basaltic units in Mare Moscoviense is re-understood using the maximum likelihood method, which suggests a different view about the mare deposits compared to the Clementine UV-VIS results and the Chandrayaan-1 M3 results.

Secondly, the T_B and dT_B performances show good correlations with the FTA distributions, especially for part of the geologic units. Through the comparison the between T_B performances in the Moscoviense Basin and those in the nearby highlands, a high substrate temperature in the Basin floor is obtained. Additionally, the T_B performances of the four units imply that the abnormally high substrate temperature likely occurs in the depth of unit Im.

Thirdly, unit Ihtm likely comprises two huge independent volcanic features based on its T_B and dT_B performances. The two highest dT_B regions are proposed as the locations of the fissures of the volcanic activities. This finding also indicates the potential significance of the CELMS data in the lunar volcanism study.

Finally, based on the dT_B performances, the highlands materials are re-evaluated. Our findings indicate that the shallow layer of the lunar crust should be homogeneous, and that there exists a low dT_B anomaly in the east highlands. We thought that the low dT_B anomaly is likely brought by a special material from the lower crust, which is still unstudied.

More work deserves to be done to further explore the CELMS data in the current lunar volcanism and composition studies.

Author Contributions: Conceptualization, Z.M. and Y.Z. (Yuanzhi Zhang); methodology, S.C. and Y.W.; software, T.W. and Z.C.; validation, Z.M., Y.Z. (Yuanzhi Zhang), and S.H.; formal analysis, Z.M.; investigation, S.C.; resources, Y.W.; data curation, Z.M. and S.C.; writing—original draft preparation, Z.M. and Y.W.; writing—review and editing, S.C., Y.Z. (Yuanzhi Zhang), and Y.Z. (Yongchun Zheng); visualization, T.W.; supervision, Z.C.; project administration, Z.M., Y.W., and Y.Z. (Yongchun Zheng); funding acquisition, S.C. and Y.Z. (Yongchun Zheng). All authors have read and agreed to the published version of the manuscript.

References

1. Wilhelms, D.E. *The Geological History of the Moon*; United States Geological Survey: Washington, DC, USA, 1987; p. 1348.

2. Gillis, J.J. The Composition and Geological Setting of Mare Deposits on the Far Side of the Moon. Ph.D. Thesis, Rice University, Houston, TX, USA, 1998.

3. Jolliff, B.L.; Gillis, J.J.; Haskin, L.A.; Korotev, R.L.; Wieczorek, M.A. Major lunar crustal terranes: Surface expressions and crust-mantle origins. *J. Geophys. Res.* **2000**, *105*, 4197–4216. [CrossRef]

4. Head, J.W. Orientale multi-ringed basin interior and implications for the petrogenesis of lunar highland samples. *Earth Moon Planet.* **1974**, *11*, 327–356. [CrossRef]

5. Ishihara, Y.; Goossens, S.; Matsumoto, K.; Noda, H.; Araki, H.; Namiki, N.; Hanada, H.; Iwata, T.; Tazawa, S.; Sasaki, S. Crustal thickness of the Moon: Implications for farside basin structures. *Geophys. Res. Lett.* **2009**, *36*, 82–90. [CrossRef]

6. Wieczorek, M.A.; Neumann, G.A.; Nimmo, F.; Kiefer, W.S.; Taylor, G.J.; Melosh, H.J.; Phillips, R.J.; Solomon, S.C.; Andrews-Hanna, J.C.; Asmar, S.W.; et al. The Crust of the Moon as Seen by GRAIL. *Science* **2013**, *339*, 671–675. [CrossRef]

7. Namiki, N.; Iwata, T.; Matsumoto, K.; Hanada, H.; Noda, H.; Goossens, S.; Ogawa, M.; Kawano, N.; Asari, K.; Tsuruta, S.; et al. Farside gravity field of the Moon from four-way Doppler measurements of SELENE (Kaguya). *Science* **2009**, *323*, 900–905. [CrossRef]

8. Gillis-Davis, J.J.; Lucey, P.G.; Hawke, B.R. Mare Moscoviense a window into the interior of the Moon. In Proceedings of the 37th Annual Lunar and Planetary Science Conference, Houston, TX, USA, 13–17 March 2006.

9. Kramer, G.Y.; Jolliff, B.L.; Neal, C.R. Distinguishing high-alumina mare basalts using Clementine UVVIS and Lunar Prospector GRS data: Mare Moscoviense and Mare Nectaris. *J. Geophys. Res. Planet.* **2008**, *113*, 769–775. [CrossRef]

10. Craddock, R.A.; Robinson, M.S.; Hawke, B.R.; McEwen, A.S. Clementine-based geology of the Moscoviense Basin, lunar farside. In Proceedings of the Lunar and Planetary Science Conference, Houston, TX, USA, 17–21 March 1997.

11. Morota, T.; Haruyama, J.; Honda, C.; Ohtake, M.; Yokota, Y.; Kimura, J.; Matsunaga, T.; Ogawa, Y.; Hirata, N.; Demura, H.; et al. Mare volcanism in the lunar farside Moscoviense region: Implication for lateral variation in magma production of the Moon. *Geophys. Res. Lett.* **2009**, *33*, 272–277. [CrossRef]

12. Thaisen, K.G.; Head, J.W.; Taylor, L.A.; Kramer, G.Y.; Isaacson, P.; Nettles, J.; Petro, N.; Pieters, C.M. Geology of the Moscoviense Basin. *J. Geophys. Res. Planet.* **2011**, *116*, E00G07. [CrossRef]

13. Pieters, C.M.; Besse, S.; Boardman, J.; Buratti, B.; Cheek, L.; Clark, R.N.; Combe, J.P.; Dhingra, D.; Goswami, J.N.; Green, R.O.; et al. Mg-spinel lithology: A new rock type on the lunar farside. *J. Geophys. Res. Planet.* **2011**, *116*, E00G08. [CrossRef]

14. Bhatt, M.; Wöhler, C.; Dhingra, D.; Thangjam, G.; Rommel, D.; Mall, U.; Bhardwaj, A.; Grumpe, A. Compositional studies of Mare Moscoviense: New perspectives from Chandrayaan-1 VIS-NIR data. *Icarus* **2008**, *303*, 149–165. [CrossRef]

15. Campbell, B.A.; Carter, L.M.; Hawke, B.R.; Campbell, D.B.; Ghent, R.R. Volcanic and impact deposits of the moon's aristarchus plateau: A new view from earth-based radar images. *Geology* **2008**, *36*, 135–138. [CrossRef]

16. Fang, T.; Fa, W.Z. High frequency thermal emission from the lunar surface and near surface temperature of the Moon from Chang'E-2 microwave radiometer. *Icarus* **2014**, *232*, 34–53. [CrossRef]

17. Meng, Z.G.; Hu, S.; Wang, T.X.; Li, C.; Cai, Z.C.; Ping, J.S. Passive microwave probing mare basalts in Mare Imbrium using CE-2 CELMS data. *IEEE J STARS* **2018**, *11*, 3097–3104. [CrossRef]

18. Meng, Z.G.; Wang, Y.Z.; Chen, S.B.; Zheng, Y.C.; Shi, J.C.; Wang, T.X.; Zhang, Y.Z.; Ping, J.S.; Hou, L.L. MTE features of Apollo Basin and its significance in understanding the SPA Basin. *IEEE J STARS* **2019**, *12*, 2575–2583. [CrossRef]

19. Lucey, P.G.; Blewett, D.T.; Jolliff, B.L. Lunar iron and titanium abundance algorithms based on final processing of Clementine ultraviolet-visible images. *J. Geophys. Res. Planet.* **2000**, *105*, 20297–20305. [CrossRef]

20. Meng, Z.G.; Zhang, J.D.; Tang, Z.S.; Ping, J.S.; Cai, Z.C. Microwave thermal emission features of Mare Orientale revealed by CELMS data. *IEEE J STARS* **2017**, *10*, 2991–2998. [CrossRef]

21. Zhu, Y.C.; Zheng, Y.C.; Fang, S.B.; Zou, Y.L.; Pearson, S. Analysis of the brightness temperature features of the lunar surface using 37 GHz channel data from the Chang'E-2 microwave radiometer. *Adv. Space Res.* **2019**, *63*, 750–765. [CrossRef]

22. Hagfors, T. Microwave Studies of Thermal Emission from the Moon. *Adv. Astronomy Astrophys.* **1971**, *8*, 1–28.

23. Keihm S, J. Effects of subsurface volume scattering on the lunar microwave brightness temperature spectrum. *Icarus* **1982**, *52*, 570–584. [CrossRef]

24. Keihm S, J. Interpretation of the lunar microwave brightness temperature spectrum: Feasibility of orbital heat flow mapping. *Icarus* **1984**, *60*, 568–589. [CrossRef]

25. Jin, Y.Q.; Yan, F.H.; Liang, Z.C. Simulation for remote sensing of the lunar soil and rock by using multi-channels microwave radiometers. *Chin. J. Radio Sci.* **2003**, *18*, 477–486.

26. Wang, Z.Z.; Li, Y.; Jiang, J.S.; Li, D.H. Lunar surface dielectric constant, regolith thickness, and ^{3}He abundance distributions retrieved from the microwave brightness temperatures of CE-1 Lunar Microwave Sounder. *Sci. China Earth Sci.* **2010**, *53*, 1365–1378. [CrossRef]

27. Heiken, G.H.; Vaniman, D.T.; French, B.M. *Lunar Sourcebook: A User's Guide to the Moon*; Cambridge University Press: London, UK, 1991.

28. Meng, Z.G.; Chen, S.B.; Edward, M.O.; Wang, Z.J.; Cui, T.F. Research on water ice content in Cabeus crater using the data from the microwave radiometer onboard Chang'e-1 satellite. *Sci. China Phys. Mech.* **2010**, *53*, 2172–2178. [CrossRef]

29. Meng, Z.G.; Wang, Q.S.; Wang, H.H.; Wang, T.X.; Cai, Z.C. Potential Geological Significances of Hertzsprung Basin Revealed by CE-2 CELMS Data. *IEEE J. STARS* **2018**, *11*, 3713–3720.

30. Cai, Z.; Lan, T. Lunar Brightness Temperature Model Based on the Microwave Radiometer Data of Chang'E-2. *IEEE Trans. Geosci. Remote* **2017**, *55*, 5944–5955. [CrossRef]

31. Meng, Z.G.; Xu, Y.; Zheng, Y.C.; Zhu, Y.C.; Jia, Y.; Chen, S.B. Inversion of lunar regolith layer thickness with CELMS data using BPNN method. *Planet. Space Sci.* **2014**, *101*, 1–11. [CrossRef]

32. Ulaby, F.T.; Moore, R.K.; Fung, A.; Feng, J.C. *Microwave Remote Sensing*; Addison-Wesley: Reading, MA, USA, 1981; pp. 51–61.

33. Jiang, J.S.; Wang, Z.Z.; Zhang, X.H.; Zhang, D.H.; Li, Y.; Lei, L.Q.; Zhang, W.G.; Cui, H.Y.; Guo, W.; Li, D.H.; et al. China probe CE -1 unveils world first Moon -globe microwave emission map-the microwave Moon some exploration results of Chang'E-1 microwave sounder. *Remote Sens. Technol. Appl.* **2009**, *4*, 409–422.

34. Meng, Z.G.; Yang, G.D.; Cai, Z.C.; Gusev, A.; Osei, E.M. Influence of (FeO+TiO$_2$) abundance on the microwave thermal emissions of lunar regolith. *Sci. China Earth Sci.* **2016**, *59*, 1498–1507. [CrossRef]

35. Chan, K.L.; Tsang, K.T.; Kong, B.; Zheng, Y.C. Lunar regolith thermal behavior revealed by Chang'E-1 microwave brightness temperature data. *Earth Planet. Sci. Lett.* **2010**, *295*, 287–291. [CrossRef]

36. Zheng, Y.C.; Tsang, K.T.; Chan, K.L.; Zou, Y.L.; Zhang, F.; Ouyang, Z.Y. First microwave map of the Moon with Chang'E-1 data: The role of local time in global imaging. *Icarus* **2012**, *219*, 194–210. [CrossRef]

37. Hu, G.P.; Chen, K.; Huang, Q.; Guo, W.; Li, Q.; Cheng, Y. Brightness Temperature Calculation of Lunar Crater: Interpretation of Topographic Effect on Microwave Data from Chang'E. *IEEE Trans. Geosci. Remote* **2014**, *52*, 4499–4510.

38. Kerle, N.; Janssen, L.L.F.; Huumeman, G.C. *Principles of Remote Sensing*; The International Institute for Geo-information Science and Earth Observation (ITC): Enschede, The Netherlands, 2009.

39. Zhu, W.Q.; Lin, W.P. *Remote Sensing Digital Image Processing*; Higher Education Press: Beijing, China, 2015.

40. Bandfield, J.L.; Ghent, R.R.; Vasavada, A.R.; Paige, D.A.; Lawrence, S.J.; Robinson, M.S. Lunar surface rock abundance and regolith fines temperatures derived from LRO Diviner Radiometer data. *J. Geophys. Res. Planet.* **2011**, *116*, E00H02. [CrossRef]

41. Blewett, D.T.; Coman, E.I.; Hawke, B.R.; Gillis-Davis, J.J.; Purucker, M.E.; Hughes, C.G. Lunar swirls: Examining crustal magnetic anomalies and space weathering trends. *J. Geophys. Res. Planet.* **2011**, *116*, E02002.

42. Meng, Z.G.; Li, X.Y.; Chen, S.B.; Zheng, Y.C.; Shi, J.C.; Wang, T.X.; Zhang, Y.Z.; Ping, J.S.; Lu, Y. Thermophysical Features of Shallow Lunar Crust Demonstrated by Typical Copernican Craters Using CE-2 CELMS Data. *IEEE J. STARS* **2019**, *12*, 2565–2574. [CrossRef]

43. Gong, X.H.; Jin, Y.Q. Diurnal change of thermal emission with "hot spots" and "cold spots" of fresh lunar craters observed by Chinese Chang'E-1. *Sci. China Inf. Sci.* **2012**, *42*, 923–935.

44. Meng, Z.G.; Wang, H.H.; Li, X.Y.; Wang, T.X.; Cai, Z.C.; Ping, J.S.; Fu, Z. Potential geological significations of Crisium Basin revealed by CE-2 CELMS data. *ISPRS* **2018**, *42*, 1279–1284. [CrossRef]

45. Arya, A.S.; Rajasekhar, R.P.; Thangjam, G.; Ajai, K.; Kumar, A.S.K. Detection of potential site for future human habitability on the moon using chandrayaan-1 data. *Curr. Sci.* **2011**, *100*, 524–529.

46. Hiesinger, H.; Head, J.W., III; Wolf, U.; Jaumann, R.; Neukum, G. Lunar mare basalt flow units: Thickness determined from crater size-frequency distributions. *Geophys. Res. Lett.* **2002**, *29*, 1248. [CrossRef]

47. Hiesinger, H.; Jaumann, R.; Neukum, G.; Head, J.W. Ages of mare basaltson the lunar nearside. *J. Geophys. Res.Planet.* **2000**, *105*, 29239–29275. [CrossRef]

48. Spudis, P.D.; Mcgovern, P.J.; Kiefer, W.S. Large shield volcanoes on the Moon. *J. Geophys. Res. Planet.* **2013**, *118*, 1063–1081. [CrossRef]

49. Pieters, C.M. Compositional diversity and stratigraphy of the lunar crust derived from reflectance spectroscopy. In *Remote Geochemical Analysis: Elemental and Mineralogical Composition*; Pieters, C., Englert, P., Eds.; Cambridge Univ. Press: Cambridge, UK, 1993; pp. 309–339.

50. Tompkins, S.; Pieters, C.M. Mineralogy of the lunar crust: Results from Clementine. *Meteorit. Planet. Sci.* **1999**, *34*, 25–41. [CrossRef]

51. Wu, Y.Z.; Xue, B.; Zhao, B.C.; Lucey, P.G.; Chen, J.; Xu, X.S.; Li, C.L.; Ouyang, Z.Y. Global estimates of lunar iron and titanium contents from the Chang'E-1 IIM data. *J. Geophys. Res. Planet.* **2012**, *117*, E02001. [CrossRef]

52. Yue, Z.Y.; Johnson, B.C.; Minton, D.A.; Melosh, H.J.; Di, K.C.; Hu, W.; Liu, Y. Projectile remnants in central peaks of lunar impact craters. *Nat. Geosci.* **2013**, *6*, 435–437. [CrossRef]

53. Meng, Z.G.; Wang, H.H.; Zheng, Y.C.; Miyamoto, H.; Cai, Z.C.; Ping, J.S. Several Geological Issues of Schrödinger Basin Exposed by CE-2 CELMS Data. *Adv. Astron.* **2019**, *2019*, 3926082. [CrossRef]

54. Meng, Z.G.; Wang, H.H.; Chen, S.B.; Ping, J.S.; Huang, Q.; Cai, Z.C.; Wu, Y.Z. Potential Geologic Issues of Von Karman Crate Revealed by Multisource Remote Sensing Data. *ISPRS* **2019**, *XLII–2/W13*, 1425–1430. [CrossRef]